

MODELING MULTI-WAVELENGTH PULSE PROFILES OF MILLISECOND PULSAR PSR B1821–24

YUANJIE DU¹, GUOJUN QIAO², PING SHUAI¹, XIAOMIN BEI¹, SHAOLONG CHEN¹, LINZHONG FU¹, LIANGWEI HUANG¹, QINGQING LIN¹, JING MENG¹, YAOJUN WU¹, HENGBIN ZHANG¹, QIAN ZHANG¹, AND XINYUAN ZHANG¹

Accepted for publication in The Astrophysical Journal

ABSTRACT

PSR B1821–24 is a solitary millisecond pulsar (MSP) which radiates multi-wavelength pulsed photons. It has complex radio, X-ray and γ -ray pulse profiles with distinct peak phase-separations that challenge the traditional caustic emission models. Using the single-pole annular gap model with suitable magnetic inclination angle ($\alpha = 40^\circ$) and viewing angle ($\zeta = 75^\circ$), we managed to reproduce its pulse profiles of three wavebands. It is found that the middle radio peak is originated from the core gap region at high altitudes, and the other two radio peaks are originated from the annular gap region at relatively low altitudes. Two peaks of both X-ray and γ -ray wavebands are fundamentally originated from annular gap region, while the γ -ray emission generated from the core gap region contributes somewhat to the first γ -ray peak. Precisely reproducing the multi-wavelength pulse profiles of PSR B1821–24 enables us to understand emission regions of distinct wavebands and justify pulsar emission models.

Subject headings: pulsars: general — pulsars: individual (PSR B1821–24) — radiation mechanisms: non-thermal — acceleration of particles

1. INTRODUCTION

PSR B1821–24 (PSR B1821–24A or PSR J1824–2452A) is a solitary energetic millisecond pulsar (MSP) first discovered in the globular cluster M28 (Lyne et al. 1987). It has a spin period $P = 3.05$ ms and a period derivative $\dot{P} = 1.62 \times 10^{-18}$ s s⁻¹ according to the ATNF Pulsar Catalogue³ (catalogue version: 1.50; Manchester et al. 2005). Due to its largest intrinsic \dot{P} (Phinney 1993), PSR B1821–24 is believed to be the most energetic MSP up to date.

PSR B1821–24 has detectable multi-wavelength emission from radio to γ -ray band. It was the first MSP with X-ray pulsed emission clearly detected by *Advanced Satellite for Cosmology and Astrophysics* (Saito et al. 1997). The X-ray pulsed emission of PSR B1821–24 has also been observed by other X-ray telescopes. At the radio band, PSR B1821–24 was the first MSP which had been observed to go through a microglitch in 2001 March (Cognard & Backer 2004). This could be a useful hint to the conventional glitch theory which should work for both young and old millisecond pulsars. Similar to other MSPs (e.g., PSR J0218+4232, PSR B1937+21 or B1957+20), PSR B1821–24 has radio giant pulses with a steep spectral index and a high degree of polarization, the phase positions of these giant pulses are overlapped with its X-ray pulses (Knight et al. 2006). In addition, Bilous et al. (2014) first presented a 720–2400 MHz phase-resolved radio measurements including polarization angle curve, spectral indices and giant pulses.

Johnson et al. (2013) showed that γ -ray, X-ray and radio pulse profiles with good signal-to-noise ratio for PSR B1821–24, which challenge the pulsar caustic models (Cheng et al. 1986; Dyks & Rudak 2003). Such models cannot self-consistently explain the complexity of its pulse profiles. PSR B1821–24 was detected to have strongly linearly polarized radio emission. With the coherently dedispersed

polarization data, Stairs et al. (1999) used the rotating vector model (RVM) to fit its polarization curve, and the inclination angle $\alpha = 40^\circ.7 \pm 1^\circ.7$ as well as the impact angle $\beta = 40^\circ \pm 10^\circ$ are derived, note that the viewing angle is $\zeta = \alpha + \beta$.

Up to date, the multi-wavelength pulse profiles of PSR B1821–24 have not been well simulated by current emission models due to its unprecedented complexity. Venter et al. (2012) speculated that PSR B1821–24 have plausible phase-aligned radio, X-ray and γ -ray pulse profiles which had not been precisely simulated. Furthermore, this pulsar does not have all peaks occurring at the same phase, according to the observed results presented by Johnson et al. (2013).

In this paper, the three-dimension annular gap model is used to study multi-wavelength (γ -ray, X-ray and radio) pulse profiles for PSR B1821–24. In Section 2, we will briefly introduce the definition of annular gap and core gap; the multi-wavelength pulse profiles for PSR B1821–24 will be simulated, and the altitudes of multi-wavelength emission will also be identified. The discussion and conclusion are shown in Section 3 and Section 4, respectively.

2. MODELING MULTI-WAVELENGTH PULSE PROFILES FOR PSR B1821–24 IN THE ANNULAR GAP MODEL

2.1. Annular Gap and Core Gap

The polar cap region of a pulsar can be divided into the annular gap and core gap regions (Du et al. 2010). In the vicinity of the light cylinder, charged particles could not co-rotate with the magnetosphere and they escaped. The pulsar must output the particles to compensate its loss. Therefore, a huge acceleration electric field (E_{\parallel}) with opposite signs are generated in both annular gap and core gap regions. This is the basic physical picture for the generation of E_{\parallel} in the annular gap model, which is suitable for both millisecond and young pulsars with short spin periods. The detailed calculations on E_{\parallel} were presented in (Du et al. 2011, 2013). A number of primary particles are accelerated to relativistic energies by E_{\parallel}

¹ Qian Xuesen Laboratory of Space Technology, NO. 104 Youyi Road, Haidian district, Beijing 100094, China; dyj@nao.cas.cn

² School of Physics, Peking University, Beijing 100871, China

³ <http://www.atnf.csiro.au/research/pulsar/psrcat/>

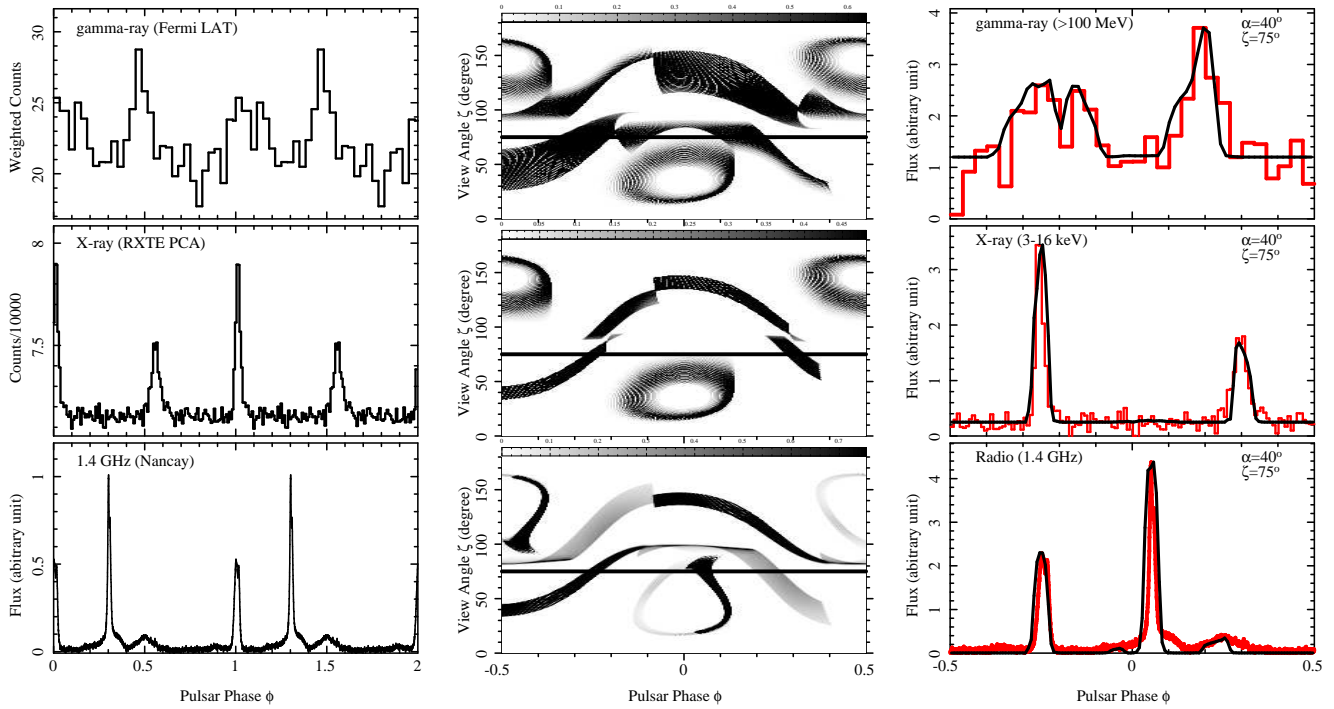


FIG. 1.— Modeled γ -ray, X-ray and radio pulse profiles for PSR B1821–24. Left panels: multi-wavelength observed pulse profile data, radio and X-ray data taken from figure 5 of Johnson et al. (2013). Middle panels: two-pole photon sky-map for an inclination angle of $\alpha = 40^\circ$. Right panels: the corresponding simulated pulse profiles (thin black solid lines) cut by only one pole emission with a viewing angle of $\zeta = 75^\circ$. The single-pole annular gap model can well reproduce the observed multi-wavelength pulse profiles (thick red solid lines in the right panels). (A color version of this figure is available in the online journal.)

in the annular and core gaps. Then the primary particles emanated a great number of γ -ray photons, most of them are converted into positron/electron pairs by the processes of γ -B and photon-photon annihilation (Du et al. 2010). Because of electron/positron pair creation, the plasma in the magnetosphere could not be fully charge-separated.

2.2. Multi-wavelength Observations

When folding γ -ray or X-ray pulse profiles of a radio-loud pulsar from *Fermi*-LAT data, a good radio timing solution is required by the TEMPO2 timing software with some relevant plugins (Hobbs et al. 2006). For PSR B1821–24, Johnson et al. (2013) presented a precise timing solution⁴ which is suitable for generating both γ -ray and X-ray pulse profiles. Using Tempo2 with the “Fermi” plugin or “photons” plugin, we were able to reproduce the γ -ray or X-ray pulse profile of PSR B1821–24. To ensure the validity of the observed pulse profiles, we directly took the γ -ray and X-ray profile data from Figure 5 of Johnson et al. (2013) (see the top and middle figure in the left panel of Figure 1). The 1.4 GHz radio profile data was taken from the webpage of “Table of Published Ephemerides” of Fermi Science Support Center. The observed pulse profiles of these three bands are then renormalized and suppressed to compare with the modeled results by the annular gap model.

The radio profile has three peaks (denoted as peak 1, peak 2 and peak 3 in turn from left to right), while the X-ray and γ -ray profiles have two main peaks (denoted as peak 1 and peak 2 from left to right) with different peak separations. The

first radio peak is almost aligned in phase with that of X-ray and γ -ray. However, the other two radio peaks have complex phase separation with comparison of the second peak of X-ray and γ -ray pulses. Johnson et al. (2013) attempted to use the outer-gap model (Cheng et al. 1986) and the two-pole caustic model (Dyks & Rudak 2003) to explain the complex features of multi-wavelength pulse profiles, but failed, then they drawn a conclusion that it would be difficult to model the actual pulse profiles across all the three wavebands. Instead, we will jointly model these three-waveband profiles in our annular gap model, and reproduce their main features including peaks and relative phase separation.

2.3. Modeling Method

§3.1 of Du et al. (2011) presented the detailed method of modeling pulse profiles. The parameterized gap width and emissivities were used, which is similar to the method usually used in the polar cap and slot gap models (Harding 2013). For both of the annular gap and core gap, we project all radiation from probable emission spots on open field lines in the emission region to the resting sky. Meanwhile, both the related aberration effect and retardation effect are considered. An assumption of Gaussian emissivities along an open field line is adopted in the modeling to speed up calculation, since this numerical assumption is consistent with physically calculated spectra in the annular gap model, as presented in Figure 8 of Du et al. (2011). Note that emissivities along different open field lines with a varying magnetic azimuthal (ψ) could be different, because the out-flowing particles on different open field lines (magnetic tubes) with different ψ could have different Lorentz factors and particle numbers. This results in a patch-like emission pattern (photon sky-map).

⁴ The timing model (par file) of PSR B1821–24 can be found at <http://fermi.gsfc.nasa.gov/ssc/data/access/lat/ephems/>.

TABLE 1
MODEL PARAMETERS OF MULTI-WAVELENGTH LIGHT CURVES FOR PSR B1821–24

Band	α	ζ	κ	λ	ϵ	ψ_{cut}	σ_{A1}	σ_{A2}	$\sigma_{\theta, A1}$	$\sigma_{\theta, A2}$	σ_C	$\sigma_{\theta, C1}$	$\sigma_{\theta, C2}$
γ -ray	40°	75°	0.94	0.8	0.8	98°	0.2	0.1	0.002	0.001	0.24	0.0025	0.0025
X-ray	40°	75°	0.84	0.8	0.8	90°	0.2	0.2	0.001	0.001	0.24	0.0025	0.0025
Radio	40°	75°	0.98	0.9	0.9	120°	0.25	0.5	0.00375	0.0025	0.4	0.0012	0.0025

The model parameters for modeling radio, X-ray and γ -ray pulse profiles of PSR B1821–24 are listed in Table 1. The model parameters are simply introduced below. α and ζ are magnetic inclination angle and viewing angle; κ and λ are two geometry parameters used to scale the peak altitude in the annular gap; ϵ is a ratio for the peak altitude in the core gap in units of the peak altitude in the annular gap; ψ_{cut} is a special magnetic azimuthal used to constrain different regions which Gaussian emissivities with different parameters are adopted; σ_{A1} and σ_{A2} are length scales in units of R_{LC} for the emission region on open field lines of $-180^\circ < \psi_s < \psi_{\text{cut}}$ and $\psi_{\text{cut}}^\circ < \psi_s < 180^\circ$ in the annular gap, respectively; σ_C is similar as σ_{A1} , but a length scale for the core gap; $\sigma_{\theta, A1}$ and $\sigma_{\theta, A2}$ as well as $\sigma_{\theta, C1}$ and $\sigma_{\theta, C2}$ are the transverse bunch scale for field lines of $-180^\circ < \psi_s < \psi_{\text{cut}}$ and $\psi_{\text{cut}}^\circ < \psi_s < 180^\circ$ in the annular gap as well as core gap, respectively. The more detailed description of these symbols is presented in (Du et al. 2011). We took the values of $\alpha = 40^\circ$ and $\zeta = 75^\circ$ which are consistent with those of the radio polarization measurement of PSR B1821–24 (Stairs et al. 1999). α and ζ are the most important parameters in our model. When they are chosen, other model parameters which stands for the emission regions are then carefully adjusted to reproduce the observed light curve of each band.

2.4. Modeling Results

The modeled multi-wavelength pulse profiles of PSR B1821–24 are well reproduced by the single-pole annular gap model, as presented in Figure 1. The corresponding emission heights for each band are shown in Figure 2. From modeling of the radio pulse, it is found that the radio emission has a non-caustic origin because of its Gaussian emissivities (see Table 1), while caustic emission tends to have a constant emissivity along an field line which is a conventional assumption as used in the two-pole caustic model (Dyks & Rudak 2003). The peak 1 and peak 3 of radio pulse originate from two regions in the annular gap with intermediate altitudes of $0.64R_{LC}$ to $0.85R_{LC}$ and $0.52R_{LC}$ to $0.78R_{LC}$, respectively; while radio peak 2 is generated in the annular gap region with higher altitudes of $0.87R_{LC}$ to $1.07R_{LC}$. For X-ray pulse, it is generated in the annular gap region located at only one magnetic pole. The emission heights of X-ray peak 1 are nearly overlapped with those of radio peak 1, while the emission region of X-ray peak 2 is $0.76R_{LC}$ to $0.98R_{LC}$, slightly higher than the heights of radio peak 3. For γ -ray pulse, the emission is also generated in the annular gap region. Peak 1 is formed by two distinct regions with altitudes of $0.36R_{LC}$ to $1.20R_{LC}$; while peak 2 originates from a region with altitudes of $0.35R_{LC}$ to $0.64R_{LC}$.

3. DISCUSSION

An observed integrated pulse profile is just a long-time accumulated photon counting (for X-rays or γ -rays) or signal

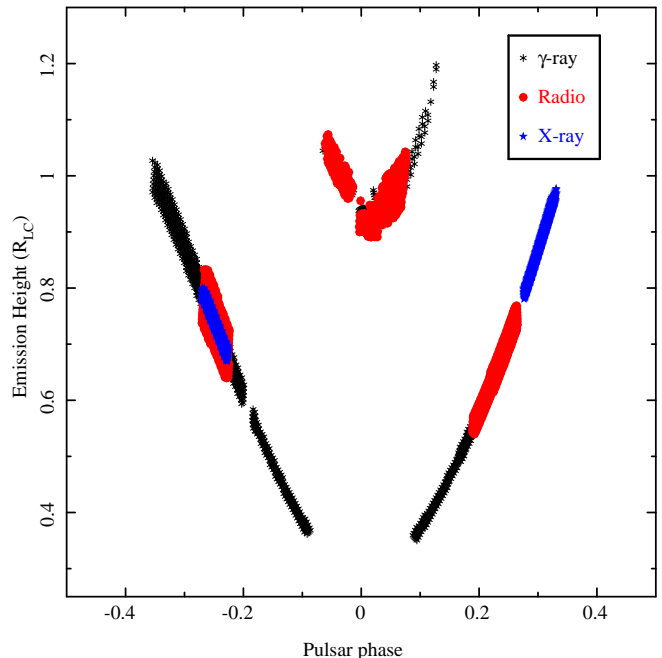


FIG. 2.— Emission heights versus phase for radio, X-ray and γ -ray pulse profiles of PSR B1821–24. It is found that shifted emission altitudes for each waveband in the single magnetic-pole, which leads to a patch-like emission pattern, can explain the complex properties of pulse profiles for PSR B1821–24.

power measurement (for radio emission) based only on a certain orientation (i.e., line of sight). It is obviously difficult to obtain the whole emission pattern on the sky for a pulsar. To maximally reproducing the multi-wavelength profiles of PSR B1821–24, the values of the most important parameters are chosen as $\alpha = 40^\circ$ and $\zeta = 75^\circ$, which are consistent with those derived from the radio polarization measurement with the RVM. As noted by Craig (2014), the effects of pulsar magnetic field configuration, emission altitude, orthogonal mode jumps, open zone radius and interstellar scattering would significantly change radio polarization properties, which results in the inaccurate values of α and ζ obtained by RVM. Particularly, the situation will be even more complex when considering the propagation effects for a radio photon in a pulsar magnetosphere (Wang et al. 2014). As a conventional method used by the two-pole caustic model and outer gap model (Dyks & Rudak 2003; Cheng et al. 2000), α and ζ are regarded as free parameters, and obtained via fitting pulse profiles. Instead, these two values here are adopted from the existing literature (Stairs et al. 1999) to be regarded as a “reference standard”, we carefully adjusted the values of α and ζ around the standard until the multi-wavelength pulse profile were reproduced. Though the final value of $\alpha = 40^\circ$ is slightly larger than the conventional values of $\alpha \lesssim 35^\circ$ presented in Du et al. (2010, 2013), but it is still in the allowable range.

Gaussian emissivities with distinct parameters for different region are also used to simulate profiles for three wavebands, in particular for the radio band. It is likely that radio emission is originated in a non-caustic emission mechanism. Radio emission from some pulsars might be generated in a incoherent style. For instance, the radio wave could be divided into ordinary mode and extraordinary mode. When they are propagating in a pulsar's magnetosphere, due to the refraction effect for the ordinary-mode wave (Wang et al. 2014), the outgoing two-mode waves are separated which leads to a incoherent and non-caustic emissivities.

We predict that other pulsars' multi-wavelength pulse profiles with complex structures (e.g. PSR J2124–3358 with four or more radio peaks) and peak separations can be well reproduced by the self-consistent annular gap model with shifted emission altitudes. Do all normal pulsars (including young and millisecond pulsars) share the same physical mechanism for radio emission? This is a long-standing question that needs a larger pulsar sample and further studies. Joint modeling both radio pulse profile and polarization angle curve with considerations of various effects discussed above

would be a valuable work which will convincingly constrain the emission geometry of a pulsar.

4. CONCLUSION

The multi-wavelength (radio, X-ray and γ -ray) pulse profiles of PSR B1821–24 can be explained by the annular gap model, and the emission region of the corresponding band are derived. The pulsed emission of all the three waveband are generated from the same magnetic pole. The shifted emission altitudes for each waveband in the single magnetic-pole, which leads to a patchy emission pattern, can account for the puzzling properties of pulse profiles for PSR B1821–24.

The authors are grateful to the referee for constructive and helpful comments. The authors are supported by the National Natural Science Foundation of China (Grant No. 11303069, 11373011 and 61403391). YJD is also sponsored by Laboratory Independent Innovation project of Qian Xuesen Laboratory of Space Technology.

REFERENCES

- Bilous, A. V., Pennucci, T. T., Demorest, P., & Ransom, S. M. 2014, arXiv:1412.7629
- Cheng, K. S., Ho, C., & Ruderman, M. 1986, *ApJ*, 300, 500
- Cheng, K. S., Ruderman, M., & Zhang, L. 2000, *ApJ*, 537, 964
- Cognard, I., & Backer, D. C. 2004, *ApJL*, 612, L125
- Craig, H. A. 2014, *ApJ*, 790, 102
- Du, Y. J., Qiao, G. J., Han, J. L., Lee, K. J., Xu, R. X. 2010, *MNRAS*, 406, 2671
- Du, Y. J., Han, J. L., Qiao, G. J., & Chou, C. K. 2011, *ApJ*, 731, 2
- Du, Y. J., Qiao, G. J., & Chen, D. 2013, *ApJ*, 763, 29
- Dyks, J., & Rudak, B. 2003, *ApJ*, 598, 1201
- Goldreich, P., & Julian, W. H. 1969, *ApJ*, 157, 869
- Harding, A. K. 2013, *Journal of Astronomy and Space Sciences*, 30, 145
- Hobbs, G. B., Edwards, R. T., & Manchester, R. N. 2006, *MNRAS*, 369, 655
- Johnson, T. J., Guillemot, L., Kerr, M., et al. 2013, *ApJ*, 778, 106
- Knight, H. S., Bailes, M., Manchester, R. N., & Ord, S. M. 2006, *ApJ*, 653, 580
- Lyne, A. G., Brinklow, A., Middleditch, J., Kulkarni, S. R., & Backer, D. C. 1987, *Nature*, 328, 399
- Manchester, R. N., Hobbs, G. B., Teoh, A., & Hobbs, M. 2005, *AJ*, 129, 1993
- Phinney, E. S. 1993, in *ASP Conf. Ser. 50, Structure and Dynamics of Globular Clusters*, ed. S. G. Djorgovski & G. Meylan (San Francisco, CA: ASP), 141
- Saito, Y., Kawai, N., Kamae, T., et al. 1997, *ApJL*, 477, L37
- Stairs, I. H., Thorsett, S. E., & Camilo, F. 1999, *ApJS*, 123, 627
- Venter, C., Johnson, T. J., & Harding, A. K. 2012, *ApJ*, 744, 34
- Wang, P. F., Wang, C., & Han, J. L. 2014, *MNRAS*, 441, 1943